Journal of Ovonic Research Vol. 10, No. 6, November - December 2014, p. 237 - 245

STUDIES ON STRUCTURAL AND OPTICAL PROPERTIES OF DC REACTIVE MAGNETRON SPUTTERED Cr DOPED CdO THIN FILMS

B. HYMAVATHI[a], B. RAJESH KUMAR[b*], T. SUBBA RAO[a]
[a]*Materials Research Lab, Department of Physics, Sri Krishnadevaray University, Anantapuramu - 515 003, A.P, India*
[b]*Department of Physics, GITAM Institute of Technology, GITAM University, Visakhapatnam -530 045, A.P, India*

Cr doped CdO thin films were deposited on mica substrates by DC reactive magnetron sputtering method by varying oxygen flow rates from 1 to 4 sccm. X-ray diffraction peaks indicates that the films were polycrystalline in nature with cubic structure. The intensity of the (2 0 0) peaks increased with the increase of oxygen flow rates. The resistivity increases from 2.12 x 10^{-4} to 5.71 x 10^{-4} Ω.cm with the increase of oxygen flow rate from 1 to 4 sccm. The carrier concentration of Cr doped CdO thin films decreases from 1.04 x 10^{20} to 0.68 x 10^{20} cm^{-3} with the increase of oxygen flow rate from 1 to 4 sccm. The optical transmittance of the thin films increases with the increase of oxygen flow rate. The optical band gap energy is varied from 2.57 to 2.69 eV with the increase of oxygen flow rate. The optical constants such as absorption coefficient (α), extinction coefficient (k) and refractive index (n) were also determined from the optical transmission data.

(Received October 26, 2014; Accepted November 29, 2014)

Keywords: Thin films; DC magnetron sputtering; X-ray diffraction; Optical transmittance

1. Introduction

Transparent conducting oxide (TCO) films like SnO_2, ZnO, In_2O_3 and CdO have been extensively studied because of their use in semiconductor device technology [1]. It is one of the promising II-VI compound semiconductors that have great potential for optoelectronic devices [2]. CdO is an interesting material because it is one of the semiconducting oxides with high carrier mobility and it has a wide range of applications in optoelectronics such as solar cells, smart windows, photo-transistors, heat mirrors and gas sensors [3]. CdO is a degenerate n-type semiconductor with electrical conductivity and transparent in visible and NIR spectral regions with a direct band gap of 2.2 - 2.7 eV[4,5]. The n-type electrical conduction in CdO is due to Cd interstitials (Cd_i) and oxygen vacancies (V_o), however the V_o is dominate defect acting as doubly ionized (+2) charge shallow donors [6]. The carrier mobility is one of the optoelectronic properties of CdO which could be controlled by doping with different metallic ions [7-11]. It was observed that dopant ions of slightly smaller size than that of Cd^{2+} improve the electronic conductivity and mobility. However, doping by using any technique of CdO with ions of much smaller radius like chromium has not yet been investigated. Chromium (Cr) doped CdO is the subject of the present study.

Various processing techniques were employed to grow CdO thin films such as reactive evaporation, sputtering deposition [12, 13], sol–gel process [14], spray pyrolysis [15], pulsed laser deposition (PLD) [16,17], molecular beam epitaxy [18], Langmuir-Blodgett deposition [19], chemical bath deposition [20], chemical vapor deposition (CVD) [21]. Among all these techniques, sputtering is considered to be the most promising techniques as this technique allows uniform film to be grown on different large-area substrates at a moderate deposition temperature.

* Corresponding author: brkhyma@gmail.com

The aim of the present work is to study the structural and optical properties of Cr doped CdO thin films prepared by DC reactive magnetron sputtering method.

2. Experimental Details

Cr doped CdO thin films were prepared by DC reactive magnetron sputtering technique. High purity of Cadmium (99.99%) and Chromium (99.99%) targets with 2 inch diameter and 4 mm thickness are used for deposition on mica substrates. The base pressure in chamber was 4.2 x 10^{-6} Torr and distance between target and substrate were set at 60 mm. High purity (99.99%) Ar and O_2 gas was introduced into the chamber and was metered by mass flow controllers for a flow rate fixed at 30 sccm for Ar and 2 sccm for O_2. Deposition was carried out at a working pressure of 2 mTorr after pre-sputtering with argon for 10 min. The DC sputtering power maintained at the time of deposition for Cd target is 100 W and 35 W for Cr target. The depositions were carried out at room temperature with different Cr concentrations. Film thickness was measured by Talysurf thickness profilometer. The resulting thickness of the films is ~300-350 nm. X-ray diffraction (XRD) patterns of the films were recorded with the help of Philips (PW 1830) X-ray diffractometer using CuKα radiation. The tube was operated at 30 KV, 20 mA with the scanning speed of 0.03(2θ)/sec. Surface morphology of the samples has been studied using HITACHI S-3400 Field Emission Scanning Electron Microscope (FESEM) with Energy Dispersive Spectrum (EDS). EDS is carried out for the elemental analysis of prepared thin film samples. Surface topography of the films has been studied using AFM (Park XE-100: Atomic Force Microscopy). The electrical resistivity of the films (ρ) was measured using the four-point probe method. Optical transmittance of the films was recorded as a function of wavelength in the range of 300 – 1200 nm using JASCO Model V-670 UV-Vis-NIR spectrophotometer (Japan).

3. Results and Discussion

Fig. 1 shows the X-ray diffraction patterns of Cr doped CdO films deposited at oxygen flow rates from 1 to 4 sccm. The presence of diffraction peaks indicates that the films were polycrystalline in nature with cubic structure. The intensity of the (2 0 0) peaks increased with the increase of oxygen flow rates. The FWHM value increases with the increase of oxygen flow rate, implies that crystallite size decreases with the increase in the oxygen flow rate. The crystallite size estimated from Scherrer formula [22] is found to be decrease from 41 to 29 nm. For a high crystallinity film, there is sufficient time for deposited atoms to undergo surface diffusion to thermodynamically stable sited before being covered by the next layer atoms. The energy of deposition flux is controlled by means of the ambient gas pressure; higher oxygen partial pressure causes lower deposition energy and small crystallite sizes; a lower oxygen partial pressure causes high deposition energy and causes large crystallite sizes. We thus speculate that this behavior is result from the energy of the deposition flux caused by the O_2 partial pressure. Thus, the crystallite size of Cr doped CdO films decreases with increasing oxygen flow rate. The lattice constant increases from 0.4705 to 0.4817 nm with the increase of oxygen flow rate from 1 to 4 sccm as shown in Fig. 2. Since the radius of Cr^{3+} is smaller than that of Cd^{2+}, the increase in the lattice constant is probably due to the incorporation of Cr atoms at the interstitial site rather than Cd site. Similar behaviour was previous reported in the literature [23].

The dislocation density (δ), defined as the length of the dislocation lines per unit volume of crystal, is evaluated using the formula,

$$\delta = \frac{n}{D^2} \tag{1}$$

where n is a factor that equals unity when the dislocation density is minimum and D is the crystallite size. The microstrain is calculated from the relation

$$\varepsilon = \frac{\beta \cos\theta}{4} \tag{2}$$

The microstrain (ε) values increased from 0.048 x 10^{-3} to 0.065 x 10^{-3} $lin^{-2}.m^{-4}$ with the increase of oxygen flow rate from 1 to 4 sccm. The dislocation density (δ) also increases from 0.60 x 10^{15} to 1.12 x 10^{15} $lin.m^{-2}$. The microstructural parameters of Cr doped CdO thin films deposited at different oxygen flow rates are tabulated in Table 1.

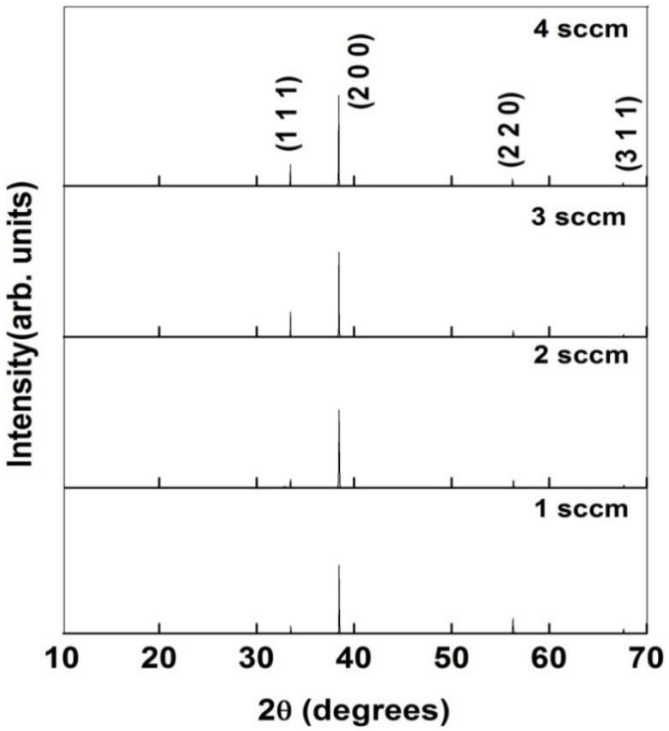

Fig. 1 XRD patterns of Cr doped CdO films deposited at various oxygen flow rates

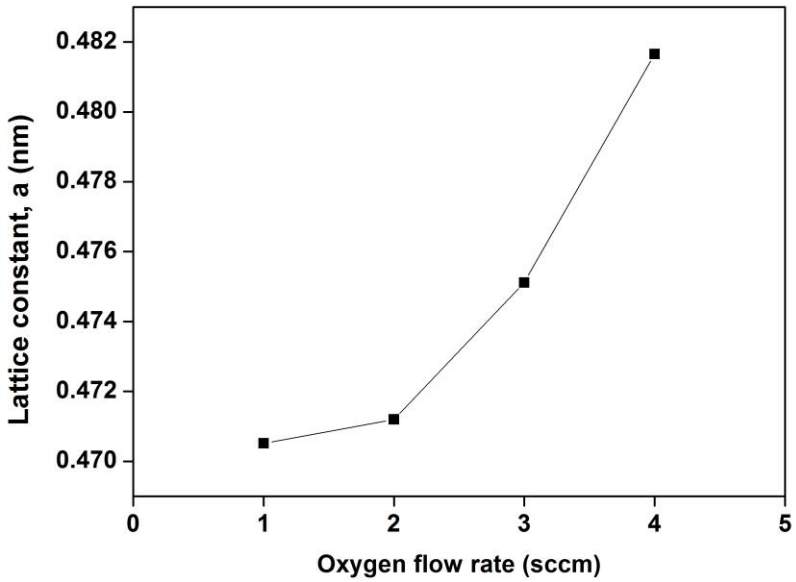

Fig. 2 Dependence of lattice constant as a function of oxygen flow rate

Table 1: Structural parameters of Cr doped CdO thin films deposited on mica substrates at various oxygen flow rates

S.No	Oxygen flow rate (sccm)	Crystallite size, D (nm)	Micro strain, ε x 10^{-3} ($lin^{-2}.m^{-4}$)	Dislocation density, δ x 10^{15} ($lin.m^{-2}$)
1	1	41	0.048	0.60
2	2	36	0.054	0.77
3	3	32	0.061	0.98
4	4	29	0.065	1.12

FESEM images of Cr doped CdO thin films of various oxygen flow rates are shown in Fig. 3. The morphology of the surface region of thin films has a crystalline columnar texture with all columnar grains oriented in the same direction and with a predominantly open micro porosity. The microstructure consists of parallel columns with gaps in between. Increasing the oxygen flow rate the columns width starts to be narrower. The grain size is found to be in the range of 24 - 42 nm for the Cr doped CdO thin films.The relative compositions obtained from EDS for Cr doped CdO films with different concentrations are in an atomic ratio of Cd/O/Cr are 59.52/37.46/3.02%, 58.86 /38.18/2.96 %, 54.18/42.78/3.04 % and 52.24/44.64/ 3.12 %.

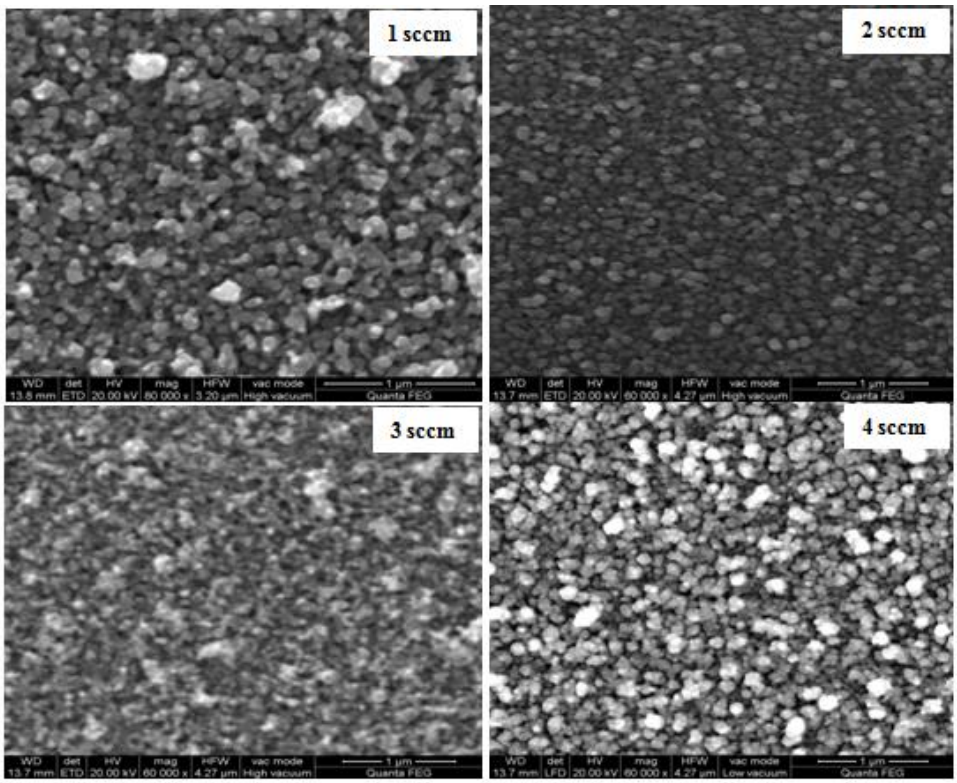

Fig. 3 FESEM images of Cr doped CdO thin films deposited at different oxygen flow rates

AFM is widely accepted as the international standard to characterize the surface roughness of a sample due to the high spatial resolution of measurement. Measuring surface roughness of Cr doped CdO thin film is important before the manufacturing of optoelectronic devices. Figure 4(a) and 4(b) shows two and three dimensional AFM images of the films deposited at oxygen flow rate

of 4 sccm with scanned over an area of 5 x 5 μm^2. AFM images indicate that the increase in the surface roughness by oxygen flow rate was caused by sharp hill-and-valley structure throughout the film surface. The average roughness and rms roughness of the Cr doped CdO films are 5.25 and 6.43 nm.

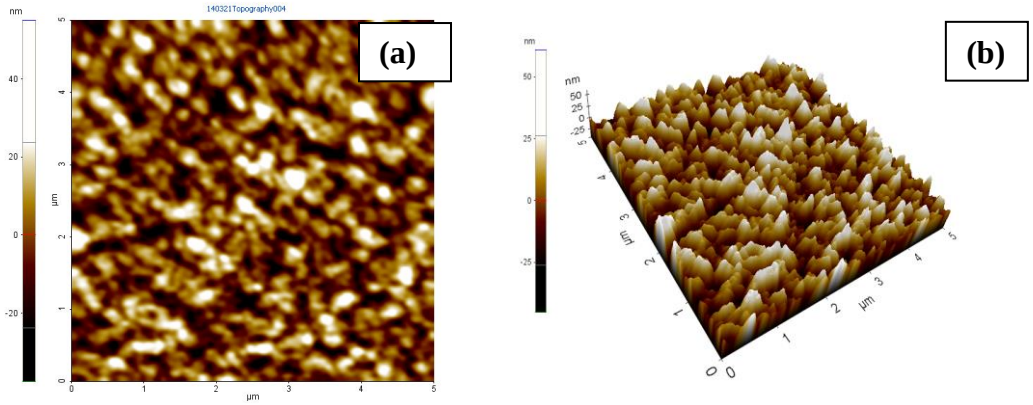

Fig. 4 (a) Two dimensional and (b) Three dimensional AFM images of Cr doped CdO thin film deposited at oxygen flow rate of 4 sccm

The electrical resistivity (ρ) of Cr doped CdO films were investigated by four-point probe method at room temperature. The resistivity increases from 2.12 x 10^{-4} to 5.71 x 10^{-4} Ω.cm with the increase of oxygen flow rate from 1 to 4 sccm shown in Fig. 5. The increase of resistivity is due to reduction of oxygen vacancies in these films. The decrease of oxygen vacancies reduces the carrier concentration resulting in increase in resistivity. The sheet resistance (R_s) of Cr doped CdO thin films are calculated from the equation

$$R_s = \frac{\rho}{t} \qquad \Omega/sq \tag{3}$$

The sheet resistance values increases with the increase of oxygen flow rate from 1 to 4 sccm. The sheet resistance values for oxygen flow rates of 1, 2, 3, and 4 sccm are found to be 6, 8.4, 11.6 and 16.3 Ω/sq respectively. The electrical parameters of Cr doped CdO thin film deposited at different oxygen flow rates are given in Table 2.

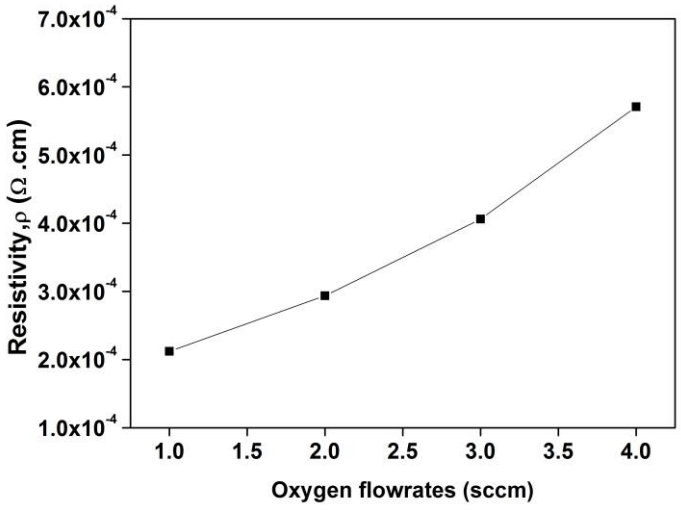

Fig. 5 Variation of electrical resistivity of the films with different oxygen flow rates

Table 2: Electrical properties of Cr doped CdO thin films

S.No	Oxygen flow rate (sccm)	Electrical resistivity, ρ (Ω.cm)	Mobility, μ ($cm^2V^{-1}s^{-1}$)	Carrier concentration, N (cm^{-3})	Sheet resistance, R_s (Ω/sq)
1	1	2.12×10^{-4}	52	1.04×10^{20}	6.0
2	2	2.93×10^{-4}	47	0.88×10^{20}	8.4
3	3	4.06×10^{-4}	38	0.72×10^{20}	11.6
4	4	5.71×10^{-4}	32	0.68×10^{20}	16.3

Fig. 6 shows the variation of Seebeck coefficient with inverse temperature for Cr doped CdO thin films deposited at different oxygen flow rates. The Seebeck coefficient values are found to be negative values indicating n-type conductivity of the films. The carrier concentration and carrier mobility of the films are determined from the equations as reported in the earlier literature [24-26]. The carrier concentration of Cr doped CdO thin films decreases from 1.04×10^{20} to 0.68×10^{20} cm^{-3} with the increase of oxygen flow rate from 1 to 4 sccm. The carrier mobility of the films decreases from 52 to 32 $cm^2V^{-1}s^{-1}$. The decrease in mobility is attributed to enhancement of oxygen release and the decrease of grain boundary scattering due to thin film densification.

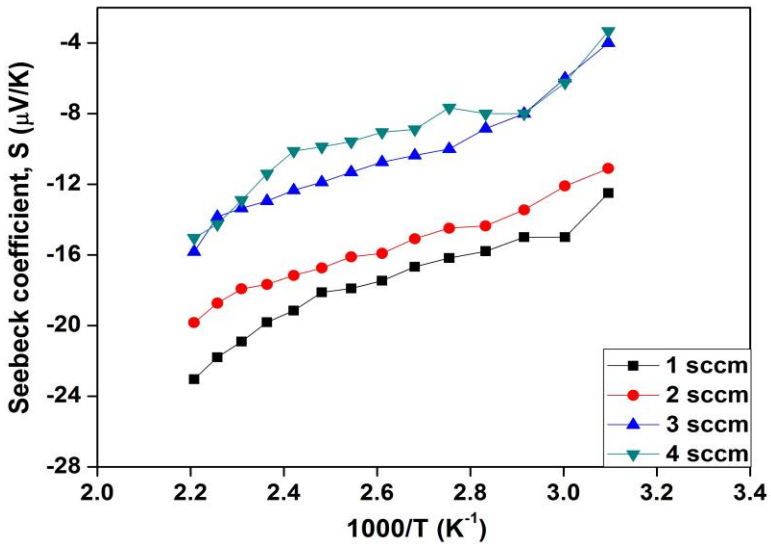

Fig. 6 Variation of Seebeck coefficient vs inverse temperature as a function of oxygen flow rates.

The optical transmittance of the films was recorded as a function of wavelength in the region of 300 - 1200 nm is shown in Fig. 7. The transmission is high in the visible region and depends on the oxygen flow rate. It is observed that the transmission of the films increased with the increase of oxygen flow rate due to decrease of density of defect centers. The light loss by the scattering of defect centers decreases as the density of defect centers decreased which results in the increase of the transmission. The absorption coefficient (α) is calculated using Lambert's law [27]

$$\alpha = \frac{\ln\left(\frac{1}{T}\right)}{d} \tag{4}$$

where T is transmittance and d is film thickness. The absorption coefficient (α) and the incident photon energy (hv) is related by the following equation [28]

$$(\alpha h\nu) = B\,(h\nu - E_g)^n \quad (5)$$

where B is a parameter that depends on the transition probability, E_g is the optical band gap energy of the material, hυ is the photon energy and n is an index that characterizes the optical absorption process and is theoretically equal to 2 and ½ for indirect and direct allowed transitions respectively. The optical band gap values were determined by extrapolating the linear portion of the plots of $(\alpha h\nu)^2$ versus hν to α = 0 as shown in Fig. 8. The optical band gap of the films increased from 2.57 to 2.69 eV with an increase in the oxygen flow rate. The increase of optical band gap may be due to the decrease of carrier concentration and due to Moss-Burstein shift [29].

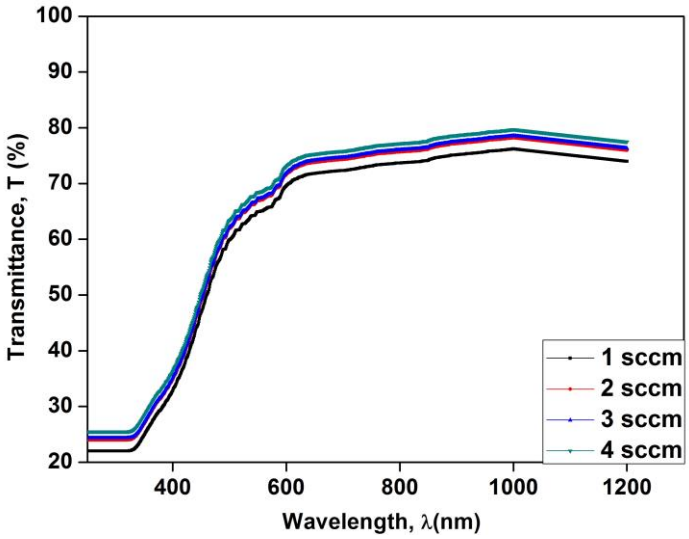

Fig. 7 Optical transmission spectra of Cr doped CdO films

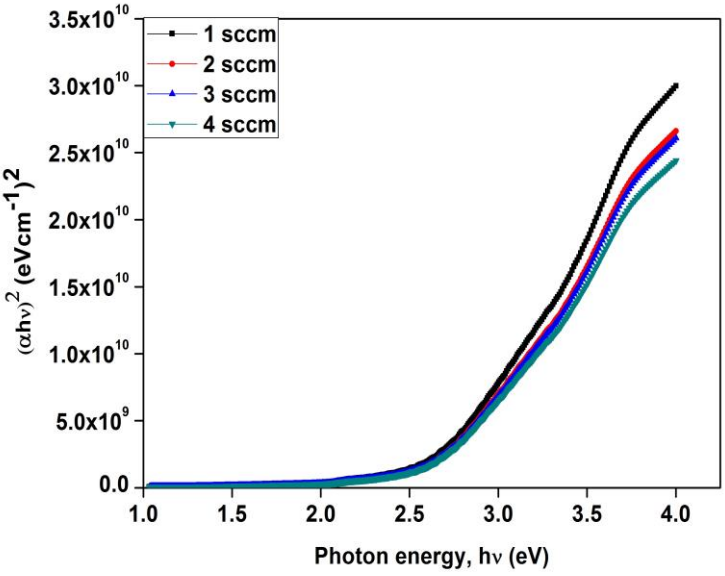

Fig. 8 Plots of $(\alpha h\nu)^2$ against photon energy (hν) of Cr doped CdO thin films

Table 3: Optical parameters of Cr doped CdO thin films deposited on mica substrates at different oxygen flow rates

S.No	Oxygen flow rate (sccm)	Absorption coefficient, α (cm^{-1})	Extinction coefficient, k	Refractive index, n	Optical band gap, E_g (eV)
1	1	8.11×10^4	0.042	2.05	2.57
2	2	8.51×10^4	0.044	2.08	2.61
3	3	8.68×10^4	0.045	2.10	2.63
4	4	9.47×10^4	0.049	2.16	2.69

The optical absorption coefficient (α) values are varied from 8.11×10^4 to 9.47×10^4 cm^{-1}. The extinction coefficient (k) values are found to be increased from 0.042 to 0.049. The refractive index of the films increased from 2.05 to 2.16 with increase of oxygen flow rate from 1 to 4 sccm. The optical properties of Cr doped CdO thin films deposited at different oxygen flow rates are tabulated in Table 3. The performance of the TCO material can be determined from the sheet resistance (R_s) and optical transmittance using figure of merit (Φ) given by Haacke's relation [30]. Generally, a film with low electrical resistivity and high optical transmittance would have a relatively high figure of merit. The figure of merit is varied from 2.7×10^{-3} to 5.7×10^{-3} Ω^{-1}. The best figure of merit with 5.7×10^{-3} Ω^{-1} is obtained for the film deposited at oxygen flow rate of 4 sccm.

4. Conclusions

Cr doped CdO films were prepared on mica substrates by varying oxygen flow rates from 1 to 4 sccm. From XRD spectra, the presence of diffraction peaks indicates that the films were polycrystalline in nature with cubic structure. The resistivity increases from 2.12×10^{-4} to 5.71×10^{-4} Ω.cm with the increase of oxygen flow rate from 1 to 4 sccm. The carrier concentration of Cr doped CdO thin films decreased from 1.04×10^{20} to 0.68×10^{20} cm^{-3} and carrier mobility of the films decreased from 52 to 32 $cm^2V^{-1}s^{-1}$with the increase of oxygen flow rate from 1 to 4 sccm. The decrease in mobility is attributed to enhancement of oxygen release and the decrease of grain boundary scattering. The highest figure of merit with 5.7×10^{-3} Ω^{-1} is obtained for the film deposited at oxygen flow rate of 4 sccm with a minimum resistivity of 5.71×10^{-4} Ω.cm and high optical transmittance of 77%. Our results suggest that the sputtered Cr doped CdO thin films can be used for optoelectronic devices.

References

[1] R.J. Deokatea, S.V. Salunkhea, G.L. Agawanea, B.S.Pawara, S.M. Pawarb, K.Y. Rajpurea, A.V. Moholkar, J.H. Kimb, J. Alloy Comp. **496**, 357 (2010).

[2] M. Benhaliliba, C.E. Benouis, A. Tiburcio-Silver, F. Yakuphanoglu, A. Avila-Garcia, A. Tavira, R.R. Trujillo, Z. Mouffack, J. Lumin. **132**, 2653 (2012).

[3] D.M. Carballeda-Galicia, R. Castanedo-Perez, O. Jimenez-Sandoval, S. Jimenez-Sandoval, G. Torres-Delgado, C.J. Zuniga-Romero, Thin Solid Films **371**, 105 (2000).

[4] Z. Zhao, D. L. Morel, C. S. Ferekides, Thin Solid Films **413**, 203 (2002).

[5] J. Santos-Cruz, G. Torres-Delgado, R. Castanedo-Perez, S. Jimenez-Sandoval, Marquez-Marin, O. Zelaya-Angel, Solar Energy **80**, 142 (2006).

[6] M. Burbano, D. O. Scanlon, G. W. Watson, J. Am. Chem. Soc. **133**,15065 (2011).

[7] Y. Dou, R. G. Egdell, T. Walker, D. S. L. Law, G. Beamson, Surf. Sci. **398**,241(1998).

[8] A. A. Dakhel, Phys. Stat. Sol. (a) **205**, 2704 (2008).

[9] R. K. Gupta, K. Ghosh, R. Patel, S. R. Mishra, P. K. Kahol, Curr. Appl. Phys.

9,673 (2009).
[10] A. A. Dakhel, Thin Solid Films **518**, 1712 (2010).
[11] R. D. Shannon, Acta Cryst. A **32**, 751 (1976).
[12] C.H.Champness, C.H.Chan, Solar Energy Mater. Solar Cells **37**, 72 (1995).
[13] F.P. Koffyberg, Phys. Rev. B **13**, 4470 (1976).
[14] A.J. Varkey, A.F. Fort, Thin Solid Films **239**, 211 (1994).
[15] R.Ferro, J.A. Rodriguez, O. Vigil, A. Moralesacevedo, G. Contraras-Puente, Phys. Stat. Sol. (a) **177**, 477 (2000).
[16] I.I. Shaganov, B.P. Kryzanovski, V.M. Dubkov, Sov. J. Opt. Technol. **48**, 280 (1981).
[17] M. Yan, M. Lane, C.R. Kannewurf, R.P.H. Chang, Appl. Phys. Lett. **78**, 2342 (2001).
[18] A.B.M.A. Ashrafi, H. Kuffmann, I. Suemune, Y.W. Ok, T.Y. Seong, Appl. Phys. Lett. **79**, 470 (2001).
[19] G. Phatak, R. Lal, Thin Solid Films **245**, 17 (1994).
[20] D.S. Dhawale, A.M.More, S.S. Latthe, K.Y. Rajpure, Mater. Sci. Eng. B **122**, 67 (2005).
[21] M. Labeau, V. Reboux, D. Dhahri, J.C. Joubert, Thin Solid Films **136**, 257 (1986).
[22] B.D. Cullity, Elements of X-Ray Diffraction, Addison-Wesley Publications Company Inc, Reading, Massachusetts (1956).
[23] F.C. Eze, Mater. Chem. Phys. **89**, 205 (2005).
[24] K. Ellmer, R. Mientus, Thin Solid Films **516,** 5829 (2008).
[25] H.L. Hartnagel, A.L. Das, A.K. Jain, C. Jagadish, Semiconducting Transparent Thin Films, Institute of Physics Publishing, Bristol (1995).
[26] L.I. Maissel, R. Glang (eds), Hand book of Thin Film technology, Mc Graw Hill Company, New York (1970).
[27] B. Joseph, P.K. Manoj, V.K.Vaidyan. Ceram. Intern. **32**, 487 (2006).
[28] J. Tauc, R. Grigorovici, A. Vancu, Phys. Stat. Sol.(b) **15**, 627 (1966).
[29] E. Burstein, Phys. Rev. **93**, 632 (1954).
[30] G. Haacke, J. Appl. Phys. **47**, 4086 (1976).